M. Wisse
A. L. Schwab

Department of Mechanical Engineering
Delft University of Technology
Mekelweg 2, 2628 CD, Delft, the Netherlands
m.wisse@wbmt.tudelft.nl

Skateboards, Bicycles, and Three-dimensional Biped Walking Machines: Velocity-dependent Stability by Means of Lean-to-yaw Coupling

Abstract

One of the great challenges in the development of passive dynamic walking robots (useful for an understanding of human gait and for future applications in entertainment and the like) is the stabilization of three-dimensional motions. This is a difficult problem due to the inherent interaction between fore–aft motions and sideways motions. In this paper we propose a simple solution. Conceptually, one can avert a sideways fall by steering in that direction, similar to skateboards and bicycles. We propose to implement this concept for walking robots by the introduction of an ankle joint that kinematically couples lean to yaw. The ankle joint has an unusual orientation; its axis points forward and downward, without any left–right component. The effect of the ankle joint is investigated in a simple three-dimensional model with three internal degrees of freedom: one at the hip and two at the ankles. It has cylindric feet and an actuator at the hip joint, which quickly moves the swing leg to a preset forward position. The simulations show that it is easy to find a stable configuration, and that the resultant walking motion is highly robust to disturbances. Similar to skateboards and bicycles, there exists a critical velocity (as a function of the parameters) above which stable walking motions occur. The critical velocity can be lower for a more vertical ankle axis orientation. As an additional benefit, the ankle joint allows a straightforward implementation for steering; a simple sideways offset of the mass distribution will cause the model to gently steer in that direction. The results show great potential for the construction of a real-world prototype with the proposed ankle joint.

The International Journal of Robotics Research
Vol. 24, No. 6, June 2005, pp. 417-429,
DOI: 10.1177/0278364905053803

KEY WORDS—passive dynamic walking, three-dimensional stability, ankle joint, simplest walking model

1. Introduction

Passive dynamic walking (McGeer 1990) is a well-known concept for the design of energy efficient bipedal (two-legged) robots with a natural-looking gait. In their purest form, such walkers are fully unactuated (and thus uncontrolled), while walking stably down a shallow slope. The swing leg moves forward at its natural frequency as a passive pendulum while the stance leg rotates forward as an inverted pendulum, usually rolling on an arc-shaped foot. For passive walkers with lateral constraints (i.e., only possessing two-dimensional (2D) dynamics) it has been shown that stable walking motions exist for a wide range of parameter values for prototypes both with and without knees. Moreover, it is straightforward to add elementary hip actuation for level-floor walking with a considerable robustness (Wisse et al. 2005) and to add an upper body through the use of a bisecting hip mechanism (Wisse, Schwab, and van der Helm 2004).

One of the great challenges is to find the key to stability in three dimensions. In addition to the fore–aft motions (pitch), in three dimensions also sideways motions (lean) and rotations around the vertical axis (yaw) are possible. It is the interaction between all three of these that renders the problem of three-dimensional (3D) stability so difficult. Consequently, most of the known solutions to this problem are successful because they reduce the interaction in one way or another, as follows:

- ignore yaw by assuming sufficient yaw resistance in the foot contact (Kuo 1999; Piiroinen 2002);

- apply large moments of inertia against yaw (Coleman and Ruina 1998; Coleman et al. 2001);
- walk with short steps (Coleman and Ruina 1998; van der Linde 2001; Tedrake et al. 2004);
- counteract yaw with a counter-rotating body (Wisse and Schwab 2001) or with counter-swinging arms (Collins, Wisse, and Ruina 2001).

In this paper, however, we aim not at a reduced interaction between the degrees of freedom, but conversely we show how a purposefully induced interaction between lean and yaw can actually benefit the stability of the walking motion.

First, in Section 2 we introduce the main idea through the related problems of skateboard and bike stability. Then, in Section 3 an elementary walking model is introduced, followed by the simulation results in Section 4 and the discussion and conclusion in Sections 5 and 6.

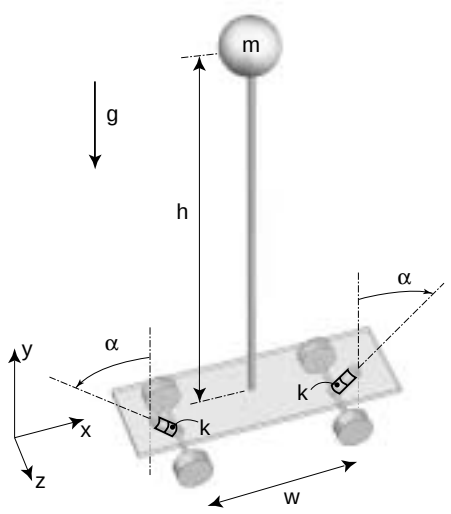

Fig. 1. Parameters of the skateboard model.

2. Advantageous Lean-to-yaw Coupling

In 3D walking, side-to-side tipping (i.e., excessive leaning) is a major stability hazard. One of the most effective control opportunities is lateral foot placement—placing the next swing leg sideways to avert a fall in that direction (Kuo 1999; Donelan et al. 2004). The key insight in this paper is that such lateral foot placement can be obtained by steering, i.e., yaw. Rotation around the vertical axis by itself has no effect, but in combination with forward progression, it suddenly affects the lateral foot placement. In other words, if during a forward walking motion one steers to the left, then automatically the next footfall will be placed more to the left side. Thus, yaw can be used for side-to-side stability, as long as there is a forward progression. Stability can be obtained if the unstable lean is either kinematically or dynamically coupled to the yaw motion.

In this section, we investigate two known examples of such advantageous lean-to-yaw coupling: a skateboard and a bicycle. These examples represent two different forms of lean-to-yaw coupling. The skateboard has a kinematic coupling; yaw and lean are combined in a single degree of freedom, as explained in Section 2.2. The bicycle has a dynamic coupling; besides the sideways lean degree of freedom of the bicycle, there is a separate degree of freedom for the steering front fork. The bicycle study is presented in Section 2.3. Note that the remainder of the paper addresses a kinematic lean-to-yaw coupling for walking machines, for which the skateboard is the most relevant analogy.

2.1. Skateboard

In the skateboard, the two sets of wheels are attached to the board via tilted steering axes (Figure 1). Although the main purpose of this construction is to give the rider the ability to steer, here we show how this also provides stability. The following analysis is a simplified version of the skateboard stability analysis by Hubbard (1979).

The board and wheels are assumed to be massless and the height between the board and the floor is neglected. Also, we assume that there is always contact between all four wheels and the floor; the model cannot tip over. The rider is modeled as a single point mass at height h above the floor, rigidly attached to the skateboard. The distance between the front and rear wheels is w. The steering axes are mounted at an angle α with respect to vertical such that sideways leaning of the rider results in steering in that direction. The steering axes are equipped with rotational springs with stiffness k. The model has fore–aft and sideways symmetry.

The skateboard is a non-holonomic system, i.e., it cannot slip sideways but it can move to a sideways position by a sequence of steering actions. Therefore, it has a smaller velocity space (lean and ride) than coordinate space (lean, x- and y-position and orientation in plane). Here we consider the linearized equations of motion in which the forward velocity can be considered as a parameter. The linearized model only has one degree of freedom, i.e., the sideways lean angle of the rider θ (Figure 2). With zero forward velocity, the behavior equals that of an inverted pendulum with a destabilizing gravity torque and a stabilizing spring torque. Although the two springs act on the tilted joints, in their projected torques the tilt angle α cancels out.

When riding with a velocity v, the skateboard makes a turn if there is a non-zero lean θ. The velocity together with the radius of curvature r_c (Figure 2) determine the sideways

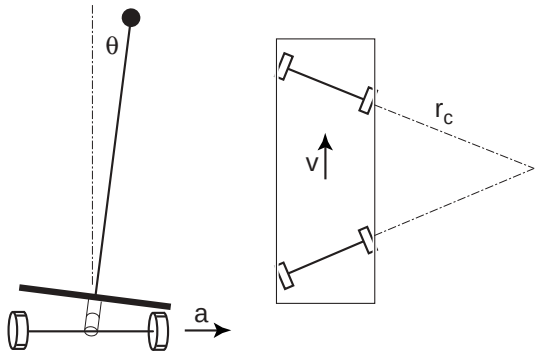

Fig. 2. Variables for the linearized skateboard model: left, a rear view; right, a top view.

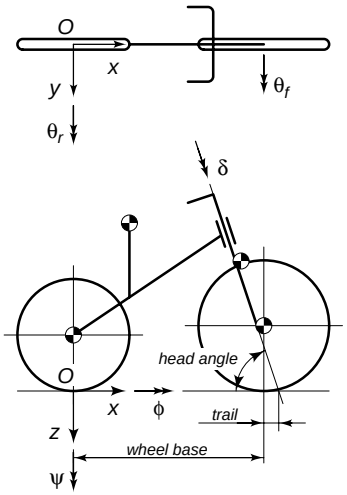

Fig. 3. Bicycle model together with the coordinate system, the degrees of freedom, and the parameters, from Schwab, Meijaard, and Papadopoulos (2005).

acceleration of the board according to

$$a = \frac{v^2}{r_c} = \frac{2v^2}{w \tan \alpha}\theta. \tag{1}$$

Therefore, the total system equation describing the linearized model becomes

$$mh^2\ddot{\theta} + \left(2k - mgh + \frac{2mh}{w \tan \alpha}v^2\right)\theta = 0. \tag{2}$$

This result can be interpreted as follows. If the spring stiffness k is high enough to counteract the inverted pendulum instability, then the system is never unstable. If not, then it can always be made stable by its velocity. The larger the angle α is, the higher the required velocity. The critical velocity is

$$v_{min} = \sqrt{\frac{(mgh - 2k)w \tan \alpha}{2mh}}. \tag{3}$$

Note that the system can at best only be marginally stable. The introduction of damping in the steering axis could make it asymptotically stable. Also note that eq. (3) suggests that it is best to make angle α equal to zero. In real life there is a lower limit to α dependent on the width of the skateboard because of the unilateral contact between the wheels and the floor.

2.2. Bicycle

Everybody knows that a bicycle is highly unstable at rest but can easily be stabilized at a moderate speed. Moreover, some uncontrolled bicycles can be asymptotically stable in a certain speed range. To demonstrate this phenomenon, we consider one of the simplest bicycle models: an uncontrolled bicycle with a rigid rider attached. This is an example of a dynamically coupled lean-to-yaw motion due to the hands-free operation of the bicycle. The following analysis is based on a recent bicycle benchmark publication by Schwab, Meijaard, and Papadopoulos (2005).

The mechanical model of the bicycle consists of four rigid bodies: the rear frame with the rider rigidly attached to it, the front frame consisting of the front fork and handle bar assembly, and the two knife-edge wheels. These bodies are interconnected by revolute hinges at the steering head between the rear frame and the front frame and at the two wheel hubs. The contact between the stiff non-slipping wheels and the flat level surface is modeled by holonomic constraints in the normal direction and by non-holonomic constraints in the longitudinal and lateral directions. There is no friction, apart from the idealized friction between the non-slipping wheels and the surface, no propulsion and no rider control, the so-called hands free coasting operation.

The mechanical model of the bicycle has three degrees of freedom: the lean angle ϕ of the rear frame, the steering angle δ, and the rotation θ_r of the rear wheel with respect to the rear frame. The forward speed is $v = -\dot{\theta}_r R_{rw}$, where R_{rw} is the radius of the rear wheel. Due to the non-holonomic constraints, there are four extra kinematic coordinates which describe, together with the degrees of freedom, the configuration of the system (Schwab and Meijaard 2003). The four kinematic coordinates are taken here as the Cartesian coordinates x and y of the rear-wheel contact point, the yaw angle ψ of the rear frame, and the rotation θ_f of the front wheel with respect to the front frame. The dimensions and mechanical properties of the benchmark model are those of a regular 18 kg bicycle with an average 76 kg rider. For the complete set of parameters, we refer to Schwab, Meijaard, and Papadopoulos (2005).

In this study, we consider the linearized model of the bicycle at constant forward speed. In the linearized model only

two degrees of freedom remain, $\mathbf{q} = (\phi, \delta)^{\mathrm{T}}$. The equations of motion are

$$\mathbf{M}\ddot{\mathbf{q}} + [\mathbf{C1} \cdot v]\dot{\mathbf{q}} + [\mathbf{K0} + \mathbf{K2} \cdot v^2]\mathbf{q} = \mathbf{f}\,, \qquad (4)$$

with a constant mass matrix, **M**, a "damping" matrix, **C1**, which is proportional to the forward speed v, and a stiffness matrix, which has a constant part, **K0**, and a part, **K2**, which is proportional to the square of the forward speed. Unfortunately the entries in the matrices are too complex and lengthy to express in a concise symbolic form. The benchmark paper (Schwab, Meijaard, and Papadopoulos 2005) does present these entries in an algorithmic manner. Simplification of these expressions by neglecting so-called minor terms, as has been done by others in the past, would lead to incorrect results. Therefore, we choose here to present typical values for the entries in the matrices, i.e.,

$$\begin{aligned}
\mathbf{M} &= \begin{bmatrix} 80.812 & 2.3234 \\ 2.3234 & 0.30127 \end{bmatrix}, \\
\mathbf{C1} &= \begin{bmatrix} 0 & 33.774 \\ -0.84823 & 1.7070 \end{bmatrix}, \\
\mathbf{K0} &= \begin{bmatrix} -794.12, & -25.739 \\ -25.739 & -8.1394 \end{bmatrix}, \\
\mathbf{K2} &= \begin{bmatrix} 0 & 76.406 \\ 0 & 2.6756 \end{bmatrix},
\end{aligned} \qquad (5)$$

where we use the standard units kg, m, and s. The forces **f** on the right-hand side are the action–reaction lean moment between the fixed space and the rear frame, and the action–reaction steering moment between the rear frame and the front frame. The latter is the torque that would be applied by a rider's hands or a controller. In the present study of an ordinary uncontrolled bicycle, both of these moments are taken to be zero.

To investigate the stability of the upright steady motion, we start from the homogeneous linearized equations of motion (4). Next we assume for the small variations in the degrees of freedom an exponential motion with respect to time, which then takes the form $\mathbf{q} = \mathbf{q}_0 \exp(\lambda t)$. This leads to an eigenvalue problem for which in this case the characteristic equation is a polynomial in the eigenvalues λ of order four. The coefficients in this polynomial are themselves polynomials in the forward speed v, since some coefficients of the linearized equations of motion have a linear or quadratic dependency on v. The solutions of the characteristic polynomial for a range of forward speeds are the root loci of the eigenvalues λ, which are shown in Figure 4. Eigenvalues with a positive real part correspond to unstable motions, whereas eigenvalues with a negative real part result in asymptotically stable motions. Complex conjugated eigenvalues give rise to oscillatory motions.

For the bicycle model there are two significant eigenmodes, called capsize mode and weave mode. The capsize motion is a non-oscillatory motion in which, when unstable, the bicycle just falls over like a capsizing ship. The weave motion is an oscillatory motion in which the bicycle sways about the headed direction. Both eigenmodes show the dynamically coupled lean-to-yaw motion. At very low speed, $0 < v < 0.7$ m s^{-1}, there are two positive and two negative eigenvalues which correspond to an inverted pendulum-like motion of the bicycle. At $v = 0.7$ m s^{-1} two real eigenvalues become identical and start forming a conjugated pair; this is where the oscillatory weave motion emerges. At first, this motion is unstable but above $v_w = 4.3$ m s^{-1} the weave motion becomes stable. After this bifurcation, the frequency of the weave motion is almost proportional to the forward speed. Meanwhile the capsize motion, which was stable for low speed, becomes mildly unstable at $v_c = 6.1$ m s^{-1}. With further increase in speed, the capsize eigenvalue approaches zero.

We conclude that the bicycle model shows a dynamic lean-to-yaw coupling resulting in an asymptotically stable motion. Similar to the skateboard, with its kinematic coupling, a minimal forward velocity is required for this stabilizing effect.

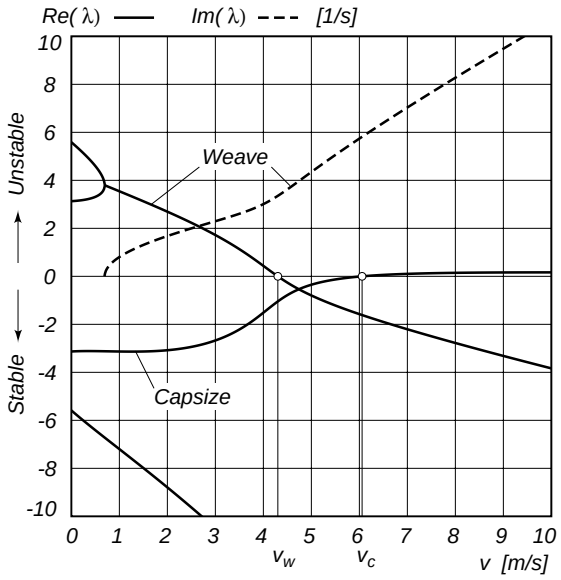

Fig. 4. Eigenvalues λ from the linearized stability analysis for the benchmark bicycle from Figure 3 and Schwab, Meijaard, and Papadopoulos (2005) where the solid lines correspond to the real part of the eigenvalues and the dashed line corresponds to the imaginary part of the eigenvalues, in the forward speed range of $0 \leq v \leq 10$ m s^{-1}. The zero crossings of the real part of the eigenvalues are for the weave motion at $v_w = 4.3$ m s^{-1} and for the capsize motion at $v_c = 6.1$ m s^{-1}, giving the bicycle an asymptotically stable speed range of $v_w < v < v_c$.

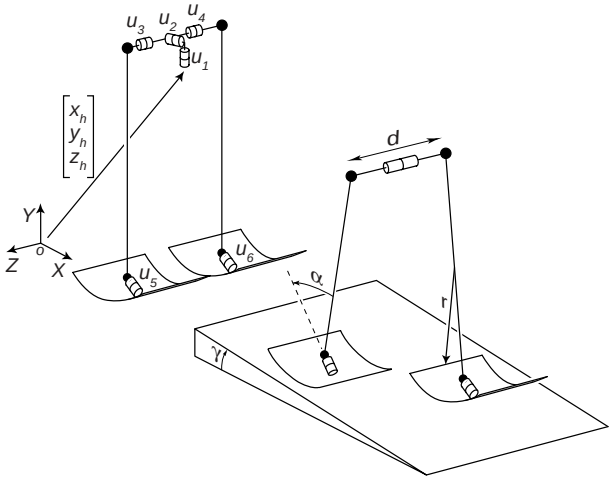

Fig. 5. Degrees of freedom (left) and parameters (right) of our simple walking model with ankle joints that couple lean to yaw.

3. Simplest Passive Walking Model with Lean-to-yaw Coupling

The purpose of the simulation model is to show the essential dynamic effects of kinematic lean-to-yaw coupling in walking systems. The simplest model for this purpose is a 3D cousin of Garcia's 2D 'simplest walking model' (Garcia et al. 1998), which consisted of one finite point mass at the hip joint, two infinitesimally small point masses at the feet, and massless rigid links in between, interconnected with a frictionless hinge at the hip. Our model (Figure 5) is a 3D extension of this; the hip has gained a finite width and the hip mass is divided into two point masses at the extremes of the massless hip axle. For numerical reasons, the point masses at the feet of our model are not infinitesimally small but just very small. The degrees of freedom are the coordinates and the yaw and lean angles of the center of the hip axle $\{x_h, y_h, z_h, u_1, u_2\}$, the two leg pitch angles $\{u_3, u_4\}$, and the two ankle angles $\{u_5, u_6\}$. The ankle axes are mounted in the x–y-plane at an angle α with respect to the vertical. Note that the ankle axes have no component in the z-direction, unlike conventional robot designs or the human ankle. The "normal" ankle functionality, rotation around the z-axis, is realized by means of the roll-off motion of the feet.

The feet are (partial) cylinder shells with the cylinder axis perpendicular to the ankle axis. They are mounted such that the cylinder axis is in the leg (not displaced forward or backward) and that the total leg length (when standing upright) is independent of the cylinder radius. The foot contact is modeled as a perfectly rigid cylinder–plane contact with only one degree of freedom: pitch in a direction perpendicular to the cylinder axis. The width of the feet is not specified and is assumed to be sufficient to prevent sideways tipping over the edge. The feet in the model have a finite size but no inertia, so the foot of the swing leg contributes to the system dynamics only as a point mass. For the detection of heel contact, the swing foot is assumed to preserve its parallel orientation with respect to the floor surface. Heel contact itself is modeled as a rigid plastic impact with immediate and full contact to the floor, while at the same instant the previous stance foot loses contact.

The model walks down a shallow slope γ. All parameters are scaled so that gravity g, the leg length l and the total robot mass ($2m_{hip}$) are all equal to one.[1] The simulation results can be scaled back to obtain results, for example, for an earthly gravity regime. This scaling exposes the minimal set of adjustable parameters: hip width d, foot radius r, ankle mounting angle α, and slope angle γ as listed in Table 1. Additionally, a (small) torque can be exerted at the hip joint to move the swing leg quickly to a forward position, a feature that will prove necessary for stable walking (Section 4).

3.1. Equations of Motion

The equations of motion for the system without foot contact constraints were generated with the method of virtual power as described in Schwab and Wisse (2001), where the 12 dependent degrees of freedom ($\{x, y, z\}$ for each point mass) were expressed in terms of the nine generalized coordinates $\{x_h, y_h, z_h, u_1 \ldots u_6\}$. In addition, there are three coordinates that change value only once per step: the foot roll-off direction ϕ and the foot contact location $\{x_c, z_c\}$. The five foot contact constraints are expressed as follows.

1. No yaw: the foot cylinder axis must remain perpendicular to its initial heading.
2. No lean: the foot cylinder axis must remain perpendicular to the normal of the floor.
3. Contact with plane: the center of the foot cylinder axis must remain a distance r (foot radius) above the floor.
4. No lateral slip.
5. No forward slip: the forward disposition should match with the pitch angle.

1. Due to the applied scaling, most quantities in this text are dimensionless, which explains the frequent use of seemingly incomplete statements such as 'a velocity of 0.36'.

Table 1. Parameters and Their Default Values

Hip width	d	0.3
Foot radius	r	0.5
Ankle mounting angle	α	0.55
Slope angle	γ	0.01

These constraint conditions (either for the right foot or for the left foot, depending on which is in stance phase) were added to the equations of motion to obtain a system of differential algebraic equations, which solves for the nine generalized coordinates and five Lagrange multipliers (one unknown contact force or torque per constraint condition). The impact equations for the heel strike event are derived in the same systematic manner (Schwab and Wisse 2001), in which the five foot contact constraints serve as contact conditions where impulsive forces can occur.

3.2. Simulation Procedure

The simulation procedure is a succession of simulations of walking steps which begin and end at the instant immediately after heel strike. Within one step, the system of differential algebraic equations is numerically integrated until heel strike is detected, followed by an impact calculation. The end state of the walker is then used as the starting state for a second step. After the second heel strike, the end state $(\{\mathbf{q}, \dot{\mathbf{q}}\}_{n+1})$ is compared to the initial state of the walker $(\{\mathbf{q}, \dot{\mathbf{q}}\}_n)$ and the entire two steps can be summarized as the non-linear stride function **S** which maps the end states on the initial states:

$$\begin{bmatrix} \mathbf{q}_{n+1} \\ \dot{\mathbf{q}}_{n+1} \end{bmatrix} = \mathbf{S}\left(\begin{bmatrix} \mathbf{q}_n \\ \dot{\mathbf{q}}_n \end{bmatrix}\right). \tag{6}$$

Note that we do not apply the common procedure of state-mirroring at the end of the step, which is used in most 2D analyses to confine the simulation to only one walking step instead of two consecutive steps.

According to the Poincaré mapping method, if the end state equals the initial state, we have found a fixed point representing a cyclic walking motion. The stability is determined by the effect of deviations $\boldsymbol{\epsilon}_n$ in the initial state on deviations $\boldsymbol{\epsilon}_{n+1}$ in the end state. For small deviations, we assume linearity around the fixed point, such that

$$\boldsymbol{\epsilon}_{n+1} = \mathbf{J}\boldsymbol{\epsilon}_n \qquad \text{with} \qquad \mathbf{J} = \frac{\partial \mathbf{S}}{\partial(\mathbf{q}_n, \dot{\mathbf{q}}_n)}. \tag{7}$$

J is the Jacobian of the stride function **S** and is determined by performing the simulation procedure once for all deviations $\boldsymbol{\epsilon}_n$, one for each independent initial condition. The stability characteristics are described by the eigenvalues $\boldsymbol{\lambda}$ of the Jacobian **J**; if all are smaller than 1 in magnitude, errors decay over subsequent strides. The smaller the eigenvalues, the faster the walker converges toward the fixed point. Note that the definition of eigenvalues here differs from Section 2; the analysis of the walking model is discrete ($-1 < \lambda < 1$ is stable) whereas the skateboard and bicycle analysis is continuous ($\lambda < 0$ is stable).

For the stability analysis, there are six relevant independent initial conditions $\{\mathbf{q}, \dot{\mathbf{q}}\}_n$ for the start of a stride. The nine independent coordinates for the free model are reduced by five foot contact constraints to four independent degrees of freedom when one foot is in contact with the floor. The angle of the swing foot is not connected to any inertia, so this leaves only three independent degrees of freedom and thus six states: $\{u_3, u_4, u_6, \dot{u}_3, \dot{u}_4, \dot{u}_6\}$ for left stance. The Poincaré section removes one state (one of the hip angles) so that there would be five independent initial conditions. In addition, there are three coordinates that change only once per step: x_c, z_c, and ϕ. The linear coordinates x_c and z_c are not relevant to the walking motion, but the foot roll-off direction ϕ is, so it must be added to the set of independent initial conditions. Therefore, in total there are six relevant independent initial conditions as listed in Table 2.

4. Simulation Results

In this section we present the behavior and stability of five simulation models of increasing complexity. The first model (Figure 6(A)) is Garcia's 2D 'simplest walking model' (Garcia et al. 1998). This fully passive model has straight legs with point feet (with infinitesimally small point masses) and a large point mass at the hip. The second model (Figure 6(B)) is similar, except that it has arc feet instead of point feet. The third model (Figure 6(C)) is equal to the second model except that it is 3D. It has no hip width but it can move out-of-plane. Also, this model is equipped with the proposed ankle joints. The fourth model (Figure 6(D)) differs in that it has a non-zero hip width, and the fifth model (Figure 6(E)) has an additional actuator at the hip joint (Wisse et al. 2004).

4.1. Fully Passive Model

Garcia et al. (1998) researched the simplest walking model in two dimensions that could still demonstrate a passive walking motion (Figure 6(A)). The model consists of three point masses, one of mass 1 at the hip and two infinitesimally small point masses at the feet, with rigid, massless links as legs interconnected with a frictionless hinge. Therefore, it has two degrees of freedom when in stance phase and thus $2\times2-1=3$ independent initial conditions for a step starting with the rear leg just leaving the floor. With its point feet (no radius of curvature), the simplest walking model is a special 2D case of the model presented in this paper.

Table 2. Fixed Point Initial Conditions for Left Stance, Valid for the Parameter Values in Table 1

Foot heading	ϕ_2	0.0016
Stance leg angle	u_4	0.155
Stance ankle angle	u_6	−0.0041
Stance leg angular velocity	$\dot{u}_4$	−0.42
Stance ankle angular velocity	$\dot{u}_6$	−0.070
Swing leg angular velocity	$\dot{u}_3$	−0.42

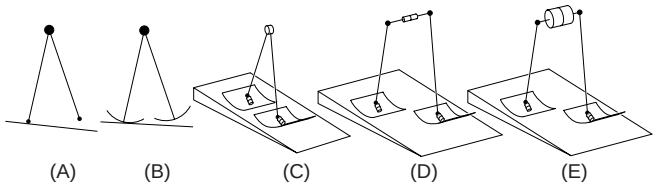

Fig. 6. Models with increasing complexity: (A) 2D point foot walker (Garcia et al. 1998); (B) 2D arc foot walker; (C) flat 3D walker (passive or active); (D) passive 3D walker with finite hip width; (E) active 3D walker.

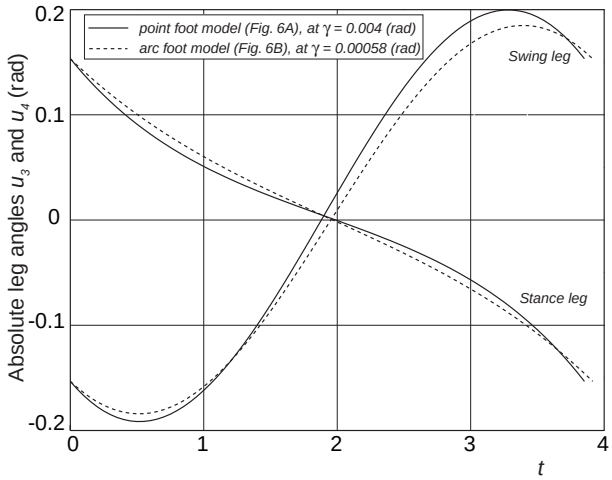

Fig. 7. Leg angles versus time for a point foot model (Figure 6(A)) and an arc foot model (Figure 6(B)) with a foot radius $r = 0.5$. The displayed cyclic walking motion (only one step is shown) is valid both for 2D models and for 3D models with zero hip width (Figure 6(C)).

The model shows a stable walking pattern when walking on a shallow slope with a downward angle smaller than 0.015 rad (Garcia et al. 1998). For example, Table 3 presents the eigenvalues $\boldsymbol{\lambda}$ for the cyclic motion that exists for a typical slope of 0.004 rad. It has been shown, however, that the simplest walking model is highly susceptible to disturbances (Schwab and Wisse 2001), and that this sensitivity can be greatly reduced by the application of arc feet with a substantial radius (Wisse and van Frankenhuyzen 2003). Therefore, we continue this paper with a model with arc feet with a radius of (a somewhat arbitrarily chosen) 0.5 times the leg length. For comparison within this paper and with previous publications (Schwab and Wisse 2001; Wisse et al. 2004), the arc foot model is given the same step length and approximately the same velocity as the point foot model by adjustment of the slope angle. The step length is determined by the initial stance leg angle θ_0. On a slope of $\gamma = 0.004$ rad, the point foot model has a limit cycle with $\theta_0 = 0.15$ rad. The arc foot walker only needs a slope of $\gamma = 0.00058$ rad for the same step length, i.e., it is about seven times more efficient while walking at the approximate same velocity (see Figure 7). The eigenvalues have moved closer to 1 and thus do not suggest a stability improvement (Table 3). However, we performed a crude analysis of the basin of attraction which showed that the arc foot walker can handle deviations from the initial conditions of 8% versus 2% for the point foot walker, indicating a better practical applicability of the model.

An interpretation of the eigenvectors corresponding to the last set of eigenvalues in Table 3 has shown that the first three eigenvalues are indeed only related to the fore–aft motions, whereas the last three eigenvalues are related to 3D motions in which both the sideways and fore–aft direction are present. The most important conclusion to be drawn from Table 3 is that there exists a stable 3D walking motion for our model with no hip width and an almost upright ankle axis ($\alpha = 0.15$ rad).

Further research shows that the eigenvalues are highly sensitive to the orientation of the ankle axis and that only a small region leads to stable motions (see Figure 8). The first three eigenvalues are not a function of the ankle axis orientation as it only influences 3D motions. The small region of stable values for α is located around the maximal stance leg angle (0.15 rad; see Figure 7). This means that, during the walking motion, the orientation of the ankle axis will move from 0.3 to 0 rad with respect to an absolute reference frame, i.e., it will have a completely vertical orientation at the end of each step. Obviously, in this orientation the ankle joint is no longer a "lean-to-yaw" coupling, but it has become a pure yaw degree of freedom. This eliminates the stabilizing effect for two reasons. First, there is no coupling so the yaw motion is not related to the rest of the walking motion, resulting in uncorrelated (and thus destabilizing) rotations around the vertical axis. Secondly, more severely, the loss of the lean degree of freedom in the ankle joint will most likely result in sideways tipping over on the inside edge of the foot, unless very wide feet are applied. Recall that a similar lower boundary exists for a realistic skateboard model.

We hypothesized that a finite hip width $d > 0$ might add to stability. A graph of the eigenvalues as a function of both the ankle orientation α and the hip width d is sketched in Figure 9. The sketch is based on a number of cross-sections in the parameter space of α and d. The stable region for α narrows down with an increasing d up to $d \approx 0.05$, beyond which no stable solutions were found for any α. A search up to $d = 0.2$ provided ever increasing eigenvalues, so we extrapolate the result to conclude that no stable 3D walking motions exist for a hip width of more than 0.05 times the leg length.

Another hypothesis was that a steeper slope might improve the stability; on a steeper slope, the passive walker will take

Table 3. Eigenvalues of the Cyclic Walking Motion for the Simplest Walking Model with Point Feet, a 2D Walker with Arc Feet, and a Flat ($d = 0$) 3D Walker with Ankle Axes Oriented at α = 0.15 rad

Eigenvalue	2D Point Foot Walker (Figure 6(A)) at $\gamma = 0.004$	2D Arc Foot Walker (Figure 6(B)) at $\gamma = 0.00058$	3D with Arc Feet (Figure 6(C)) at $\gamma = 0.00058$
λ_1	$-0.3 + 0.27i$	0.69	0.69
λ_2	$-0.3 - 0.27i$	0.12	0.12
λ_3	0	0	0
λ_4	–	–	0.72
λ_5	–	–	0.51
λ_6	–	–	0

Note that all eigenvalues result from two successive steps, i.e., one stride.

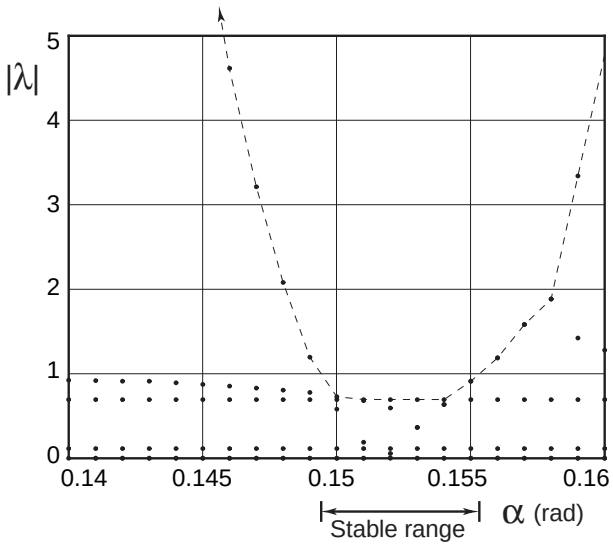

Fig. 8. Typical plot of the absolute values of the eigenvalues $|\lambda|$ as a function of the ankle joint orientation α for a fully passive 3D model (Figure 6(C)). This plot is generated with hip width $d = 0$ and foot radius $r = 0.5$, walking on a slope of $\gamma = 0.00058$ rad.

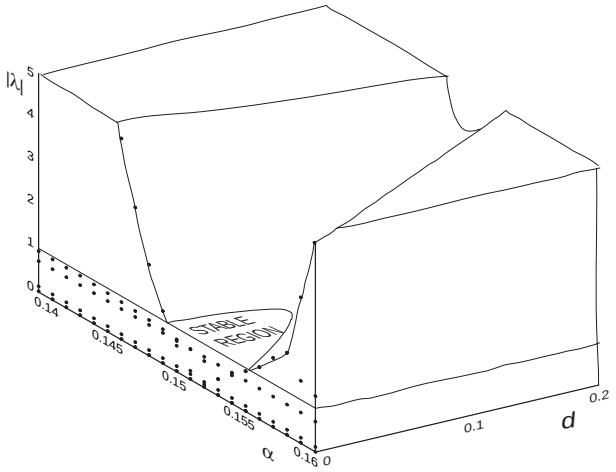

Fig. 9. A sketch of the dependency of the eigenvalues as a function of ankle joint orientation α and hip width d for a model (Figure 6(D)) with foot radius $r = 0.5$ and slope angle $\gamma = 0.00058$ rad. The left face of the figure is equal to Figure 8.

larger steps and thus walk faster, and the skateboard and bike models predict a beneficial stability effect for higher velocities. However, the simulation has shown only marginal effects. Up to the maximal slope of 0.046 rad beyond which no stable motions exist, the 3D graph in Figure 9 remains similar in shape. The stable region shifts to higher values of α along with the increase in step length. For example, a slope increase from 0.00058 to 0.004 rad causes the initial stance leg angle to increase from 0.15 to 0.29 rad and also shifts the stable values for α from around 0.15 to around 0.29 rad.

These marginal stability results, together with the required vertical orientation of the ankle axis, indicate that the fully passive model is not sufficiently applicable for real-world prototypes, and warrant a search for a model with stable behavior for larger values of α and d.

4.2. Model with Hip Actuation

In this subsection we propose to improve the overall (3D) walking behavior through the addition of a stabilizing feature that was originally intended for 2D machines. In two dimensions, the most persistent failure is a fall forward, which can be averted by simply accelerating the swing leg to bring it

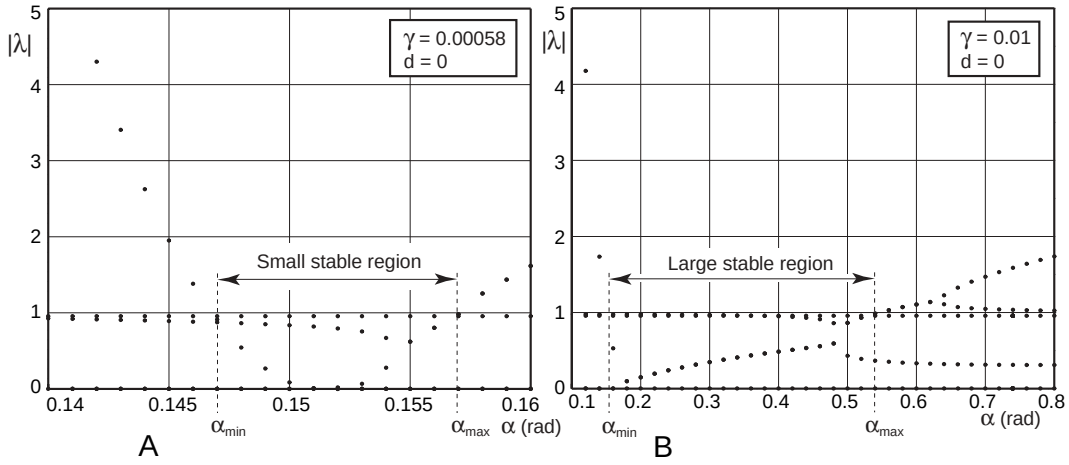

Fig. 10. Typical plot of the absolute values of the eigenvalues $|\lambda|$ as a function of the ankle joint orientation α for a 3D model with simple swing leg control (Figure 6(C)). This plot is generated with hip width $d = 0$ and foot radius $r = 0.5$, walking on a slope of $\gamma = 0.00058$ rad (left) and $\gamma = 0.01$ rad (right). The two graphs exemplify that the upper boundary for α increases with an increasing γ; the steeper the slope, the larger the region of stability. Note the difference in scale of the two graphs.

quickly to a forward position and subsequently keeping it there (Wisse et al. 2004). This simple form of swing leg control can be implemented on our 3D model without energy implications; the swing leg is nearly massless, so any control action can be applied (almost) without reaction torques to the rest of the model. Therefore, the model still requires a downhill slope for a sustained walking motion. This also means that the swing leg can be moved arbitrarily fast; in the remainder of this paper, the swing leg is assumed (and simulated) always to be in the forward position before heel strike occurs.

We can arbitrarily set the forward angle that the swing leg is quickly moved to. Let us maintain the value of 0.15 rad as initial stance leg angle in accordance with the passive models described earlier. The controller therefore has to move the swing leg quickly to an inter-leg angle of $2 \times 0.15 = 0.3$ rad. The immediate effect of the controller is that disturbances on the initial swing leg velocity do not affect the end state, and thus one of the eigenvalues of the model becomes zero.

Looking at the behavior for $\gamma = 0.00058$, there seems to be little difference between the active model (Figure 10(A)) and the passive model (Figure 8). The reason is that the main improvements are to be found for larger slopes. For the active model, a change of slope does not lead to a change of step length, while the swing leg control ensures that the model cannot fall forward, so any arbitrarily steep slope can be used. These two effects of the swing leg control together result in a much more favorable behavior. In contrast to the passive model, for the active model an increase of γ does not lead to a translation of the stable region for α but rather to an increase of this region, shown in Figure 10(B).

The stable region in Figure 10(B) has two independent boundaries. The lower boundary for α is directly related to the step length; if α is lower than 0.15, the ankle axis would reach a vertical orientation at the end of the step which leads to directional instability. With a fixed step length due to the swing leg controller, this lower boundary for α is more or less static. The upper boundary is directly related to the slope angle; the steeper the slope, the higher α can be. Or, in other words, for a given value of α the slope angle must be above a certain critical value for stable walking. In Figure 11 this is depicted for $\alpha = 0.55$, the upper boundary from Figure 10(B). Note the correlation between the two graphs; the upper boundary $\alpha = 0.55$ in Figure 10(B) corresponds to the stability boundary $\gamma = 0.01$ in Figure 11.

With respect to the passive model, the active model has a much larger stable region; when walking on a slope of $\gamma = 0.01$ rad, the ankle orientation angle can be anything between $0.15 < \alpha < 0.55$ rad for stable walking. This gives good hopes for models with a finite hip width. Figure 12 presents the eigenvalues as a function of both α and the hip width d, where the left front plane equals Figure 10(B). Apparently, for the active model an increase of the hip width is even beneficial to the stability, in sharp contrast with the passive model.

4.3. Stability Versus Velocity

For the active model, it is easy to find a parameter combination that results in stable walking. Figure 11 basically suggests that for any parameter combination, one can find stability by increasing the slope angle past a critical value. This effect

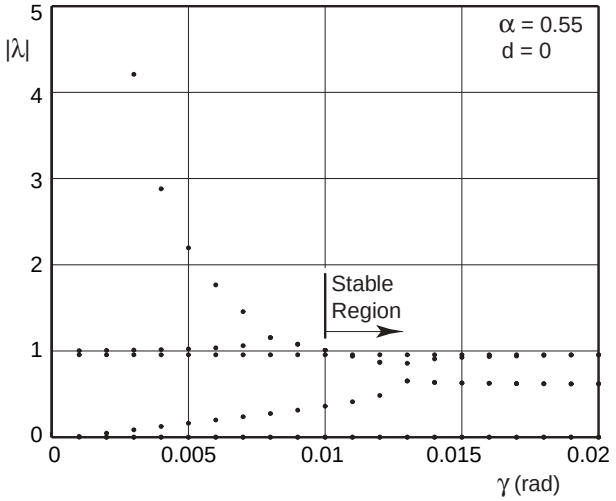

Fig. 11. Typical plot of the absolute values of the eigenvalues $|\lambda|$ as a function of slope angle γ for a 3D model with simple swing leg control (Figure 6(C)). This plot is generated with hip width $d = 0$, a foot radius $r = 0.5$, and an ankle joint orientation $\alpha = 0.55$ rad. For $\gamma > 0.01$, the model is stable. This boundary corresponds to the upper stability boundary in the right graph of Figure 10.

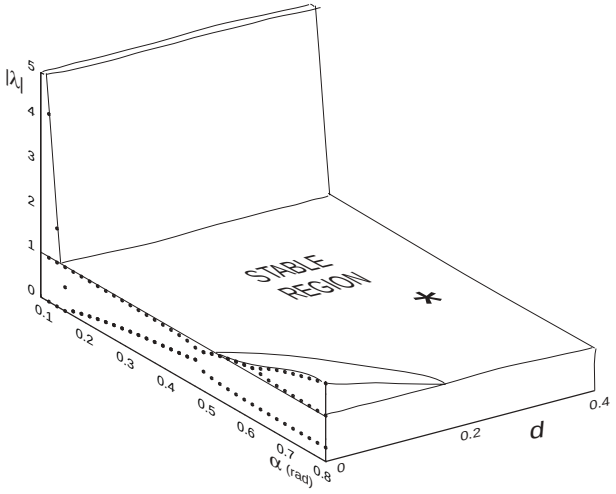

Fig. 12. Sketch of the eigenvalues of the active model as a function of ankle joint orientation α and hip width d for a model (Figure 6(E)) with foot radius $r = 0.5$ and slope angle $\gamma = 0.01$ rad. The left face is equal to the right graph of Figure 10. The asterisk indicates the parameter set of Table 1.

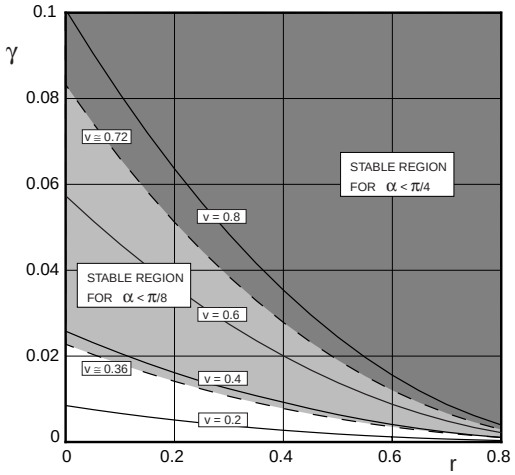

Fig. 13. Stability regions and walking velocity as a function of the slope angle γ and the foot radius r for an active, flat 3D model (Figure 6(C)). The velocity is determined by the parameters r and γ and is independent of α. The stability is dependent on all three parameters. The graph shows that a more vertical ankle axis (smaller α) provides stability for lower velocities. Interestingly, the stability boundaries are almost completely coincident with lines of constant velocity; the (dashed) boundary of the (light gray) stability region for $\alpha < \pi/8$ is almost exactly equal to the line of constant velocity for $v = 0.36$ (not shown). Similarly, the (dashed) boundary of the (dark gray) stability region for $\alpha < \pi/4$ is almost exactly equal to $v = 0.72$ (not shown). Therefore, we conclude that stability can be seen as a function of the velocity independent of the particular slope and foot radius that cause the velocity. Note that the velocity lines are obtained with the numerical simulation, not with the algebraic approximation in eq. (8).

has the same feel to it as the velocity relation in skateboards and bicycles, in which for most parameter values there exists a critical velocity above which stable motions occur. Therefore, it is interesting to investigate the relation between the slope angle, the walker's velocity, and its stability, to answer the question: is there a direct relationship between velocity and stability?

To answer this question, we need to bring r into the equation because the velocity is determined by γ and r for a given step length. For manageability of the model and calculations, we answer this question only for the flat version of the 3D model, i.e., $d = 0$ (Figure 6(C)). The result is stunning; according to Figure 13 there is almost a one-to-one relationship between the velocity and the stability, irrespective of the specific values of r and γ that cause that velocity.

The result in Figure 13 was obtained as follows. First, the plot contains contour lines of constant velocity. The walking

velocity is a result of the gravitational energy input and the energy loss at the heel strike impact, which are in balance when the walker is in a limit cycle. An analysis of the energy balance (not shown here for brevity) leads to the following approximate relationship

$$v \approx \frac{1}{(1-r)}\sqrt{\frac{\gamma}{\theta}} \tag{8}$$

where v is the walking velocity and θ is the stance leg angle at the start of the step (equal to half of the preset inter-leg angle). This approximation ignores the velocity decrease at mid-stance and therefore slightly overestimates the walking velocity. Equation (8) clearly shows that if r equals the leg length 1, then the walker could have any velocity at a slope of 0 while no equilibrium exists for any other slope angle, because no energy is lost during heel strike. In Figure 13 we used the exact velocities (from the non-linear simulations) rather than the approximation in eq. 8.

The second ingredient of Figure 13 is the shape of the region of stability. The figure shows for two different values of the ankle joint orientation α what combinations of values for the slope angle γ and the foot radius r lead to stable walking. The figure shows what was already known from Figure 10; a steeper slope (larger γ) allows for a more horizontal ankle joint (larger α). The additional information in Figure 13 is how the stability boundary depends on both γ and r, which apparently coincides with contour lines of constant velocity. An heuristic formula for the boundary value of α as a function of the velocity v can easily be extracted from the data scattered in this paper. From Figures 10 and 13 we can extract four data points that show an almost one-to-one linear relationship, $v_{min} \approx \alpha$.

4.4. Walking and Steering

The previous subsections have shown that it is easy to find stable parameter combinations for the active model. In this subsection we investigate the resultant walking motion for one characteristic set of parameter values (Table 1).

For a steady walk, the projection of the center of mass and the footprints are shown in Figure 14. The step length of 0.3 times the leg length is a direct result of the swing leg controller. The center of mass makes sideways excursions of ± 0.008 times the leg length.

The model's inherent stability means that it will react to any (not too large) disturbance by asymptotically moving back to its steady limit cycle. This fact can be used for intentional steering; if the model were placed on the slope in a direction other than steepest descent, it will automatically steer toward that direction. Or, even more useful, a sideways mass offset will also induce steering in that direction. In Figure 15, which contains a sequence of 500 walking steps, the center of mass was displaced slightly (0.006 times the leg length) to the right. The result is that the model asymptotically moves toward a heading direction of 0.64 rad with respect to the direction of steepest descent. With its new heading, the model has found balance between the mass offset to the right and the offset effect of the slope to the left.

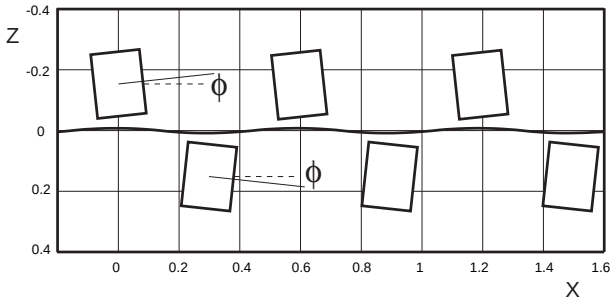

Fig. 14. Projection of the center of mass on the floor together with footprints for the full model (Figure 6(E)). The grid on the floor is in units of leg length. The model walks from left to right in a steady motion. The footprint direction ϕ is exaggerated; the true value $\phi = 0.00155$ (see Table 2) would be invisible in the figure.

The model is robust enough to handle a much larger mass offset. Even if the center of mass is sideways displaced with 0.05 times the leg length, a steady (although somewhat limping) walking motion exists. With this offset, the model will turn with a radius of about eight times the leg length, as shown with the dashed line in Figure 15. It stops and falls not because of the direct effect of the mass offset, but because it has turned more than 90° and thus receives no energy input. If the slope would turn with the walker, it would walk indefinitely in circles.

As a final stability test we investigated the disturbance rejection of the model. The model was started with the initial conditions for the steady walking motion plus an error on one of them. The model is able to recover from an increase of at least 200% or a decrease of 100% on any of the initial conditions, except for the velocity of the stance leg angle. The stance leg's angular velocity can only be decreased with 50%, otherwise the model falls backward. All in all, the model predicts great potential for practically applicable prototypes.

5. Discussion

The simulations predict successful walking for prototypes with the special ankle joint that couples falling sideways (lean) to turning in that direction (yaw). The solution to any instability is to increase the walking velocity. There is however a practical limit to the walking velocity. The simulation assumes that the (almost massless) swing leg is always in time to catch the walker for its next step, but a physical swing leg with substantial mass cannot move instantaneously. Its

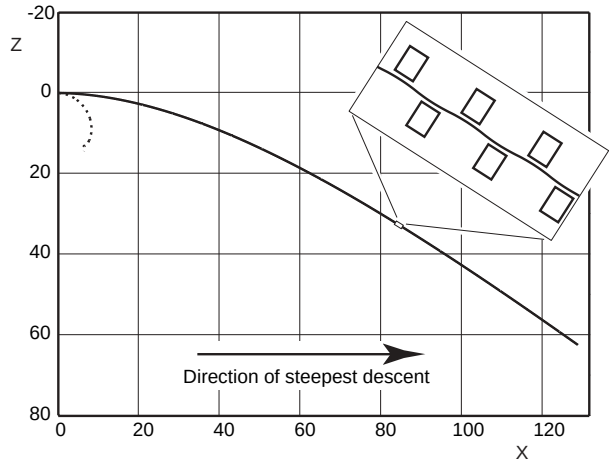

Fig. 15. Projection of the center of mass on the floor together with footprints for 500 steps. The model has a mass offset to the right and thus steers asymptotically toward a direction in which the sideways slope effect is in balance with the effect of the mass offset. A much larger mass offset results in a tighter turn as shown with the dashed line. After a turn of more than 90°, the walker receives no energy input and eventually stops and falls.

velocity is not only limited by practical considerations (actuator capacity), but also by the fact that its reaction torque might exceed the friction torques that the stance foot can supply.

Our model is not equipped with springs in the ankle joints for the sake of simplicity. The skateboard analysis, however, predicts a beneficial influence of such springs. It is recommended for future research to investigate the possible stability benefit that such springs can provide for walking robots.

The implication of this paper for the creation of stable prototypes goes beyond the concept of the tilted ankle joint. Even if the proposed ankle joint is not implemented in a prototype, it is still possible to benefit from the idea behind it; any control algorithm anywhere in the body can have similar beneficial stability effects, as long as its effect is a lean-to-yaw coupling. We expect that such an effect is also present in the human body, albeit well masked by the simultaneous presence of two other control strategies for sideways stability: sideways foot placement (Bauby and Kuo 2000; Donelan, Kram, and Kuo 2001; Donelan et al. 2004) and inertial reaction torques from the upper body.

In the future, we hope to gain more insight into the similarity between a kinematic lean-to-yaw coupling as studied in this paper, and a dynamic coupling as presented in the bicycle example. A promising lead is the stable walking behavior that was found in a 3D rimless wheel (Coleman, Chatterjee, and Ruina 1997). Another lead is provided by Kuo (1999) who found that lateral stability can be obtained through fore–aft leg motions, which should also be considered as a dynamic lean-to-yaw coupling.

6. Conclusion

This paper shows that a special ankle joint that couples falling sideways (lean) to turning in that direction (yaw) can lead to stable 3D walking models. A practical robustness against disturbances requires a basic form of swing leg control, which moves the swing leg quickly to a forward position. With this control rule in place, the model shows behavior that corresponds to bicycles and skateboards; stable motions exist above a certain critical forward velocity, depending on the tilt angle α of the ankle axis. The more vertical the axis (smaller α), the lower the critical velocity. There is a minimum, however; the tilt angle α must always remain larger than the maximal stance leg angle, otherwise it would have a completely vertical orientation at the end of a step. This not only leads to instabilities but also requires impractical wide feet to prevent tipping over on the inside of the foot.

The ankle joint provides an effective means for direction control; a slight asymmetry in any of the parameters (such as a sideways mass offset) results in a walk on a curved path. The simulations with the elementary model presented in this paper predict a sufficient robustness against disturbances to warrant the construction of a physical 3D prototype.

Acknowledgment

This research is partially funded by the Dutch National Technology Foundation (STW).

References

Bauby, C. E. and Kuo, A. D. 2000. Active control of lateral balance in human walking. *Journal of Biomechanics* 33:1433–1440.

Coleman, M. J. and Ruina, A. 1998. An uncontrolled toy that can walk but cannot stand still. *Physical Review Letters* 80(16):3658–3661.

Coleman, M. J., Chatterjee, A., and Ruina, A. 1997. Motions of a rimless spoked wheel: a simple 3D system with impacts. *Dynamics and Stability of Systems* 12(3):139–160.

Coleman, M. J., Garcia, M., Mombaur, K., and Ruina, A. 2001. Prediction of stable walking for a toy that cannot stand. *Physical Review E* 64(2):022901-1–022901-3.

Collins, S. H., Wisse, M., and Ruina, A. 2001. A two-legged kneed passive dynamic walking robot. *International Journal of Robotics Research* 20(7):607–615.

Donelan, J. M., Kram, R., and Kuo, A. D. 2001. Mechanical and metabolic determinants of the preferred step width

in human walking. *Proceedings of the Royal Society of London B* 268:1985–1992.

Donelan, J. M., Shipman, D. W., Kram, R., and Kuo, A. D. 2004. Mechanical and metabolic requirements for active lateral stabilization in human walking. *Journal of Biomechanics* 37:827–835.

Garcia, M., Chatterjee, A., Ruina, A., and Coleman, M. J. 1998. The simplest walking model: stability, complexity, and scaling. *ASME Journal of Biomechanical Engineering* 120(2):281–288.

Hubbard, M. 1979. Lateral dynamics and stability of the skateboard. *Journal of Applied Mechanics* 46:931–936.

Kuo, A. D. 1999. Stabilization of lateral motion in passive dynamic walking. *International Journal of Robotics Research* 18(9):917–930.

McGeer, T. 1990. Passive dynamic walking. *International Journal of Robotics Research* 9(2):62–82.

Piiroinen, P. T. 2002. Recurrent dynamics of non-smooth systems with application to human gait. Ph.D. Thesis, Royal Institute of Technology, Stockholm, Sweden.

Schwab, A. L. and Meijaard, J. P. 2003. Dynamics of flexible multibody systems with non-holonomic constraints: a finite element approach. *Multibody System Dynamics* 10(12):107–123.

Schwab, A. L. and Wisse, M. 2001. Basin of attraction of the simplest walking model. *Proceedings of the ASME Design Engineering Technical Conferences*, Pittsburgh, PA, Paper number DETC2001/VIB-21363.

Schwab, A. L., Meijaard, J. P., and Papadopoulos, J. M. 2005. Benchmark results on the linearized equations of motion of an uncontrolled bicycle. *KSME Journal of Mechanical Science and Technology* 19(1):292–304.

Tedrake, R., Zhang, T. W., Fong, M-F., and Seung, H. S. 2004. Actuating a simple 3D passive dynamic walker. *Proceedings of the IEEE International Conference on Robotics and Automation (ICRA)*, New Orleans, LA.

van der Linde, R. Q. 2001. Bipedal walking with active springs, gait synthesis and prototype design. Ph.D. Thesis, Delft University of Technology, Delft, the Netherlands, November.

Wisse, M. and Schwab, A. L. 2001. A 3D passive dynamic biped with roll and yaw compensation. *Robotica* 19:275–284.

Wisse, M. and van Frankenhuyzen, J. 2003. Design and construction of Mike: a 2D autonomous biped based on passive dynamic walking. *Proceedings of the Conference on Adaptive Motion of Animals and Machines (AMAM)*, Kyoto, Japan, Paper number WeP-I-1.

Wisse, M., Schwab, A. L., and van der Helm, F. C. T. 2004. Passive dynamic walking model with upper body. *Robotica* 22:681–688.

Wisse, M., Schwab, A. L., van der Linde, R. Q., and van der Helm, F. C. T. 2005. How to keep from falling forward: elementary swing leg action for passive dynamic walkers. *IEEE Transactions on Robotics* in press.